

Accepted Manuscript

Title: Probing the synergistic effect of Mo on Ni-based catalyst in the hydrogenation of dicyclopentadiene

Authors: Zhuqing Fang, Daxin Shi, Na Lin, Airu Li, Qin Wu, Qiqi Wang, Yun Zhao, Caihong Feng, Qingze Jiao, Hansheng Li



PII: S0926-860X(19)30042-0
DOI: <https://doi.org/10.1016/j.apcata.2019.01.026>
Reference: APCATA 16966

To appear in: *Applied Catalysis A: General*

Received date: 6 November 2018
Revised date: 9 January 2019
Accepted date: 29 January 2019

Please cite this article as: Fang Z, Shi D, Lin N, Li A, Wu Q, Wang Q, Zhao Y, Feng C, Jiao Q, Li H, Probing the synergistic effect of Mo on Ni-based catalyst in the hydrogenation of dicyclopentadiene, *Applied Catalysis A, General* (2019), <https://doi.org/10.1016/j.apcata.2019.01.026>

This is a PDF file of an unedited manuscript that has been accepted for publication. As a service to our customers we are providing this early version of the manuscript. The manuscript will undergo copyediting, typesetting, and review of the resulting proof before it is published in its final form. Please note that during the production process errors may be discovered which could affect the content, and all legal disclaimers that apply to the journal pertain.

Probing the synergistic effect of Mo on Ni-based catalyst in the hydrogenation of dicyclopentadiene

Zhuqing Fang^a, Daxin Shi^{a*}, Na Lin^b, Airu Li^a, Qin Wu^a, Qiqi Wang^a, Yun Zhao^a, Caihong Feng^a, Qingze Jiao^{a, c}, Hansheng Li^{a*}

^a School of Chemistry and Chemical Engineering, Beijing Institute of Technology, Beijing 100081, China.

^b School of Materials Science and Engineering, Beijing Institute of Technology, Beijing 100081, China.

^c School of Materials and Environment, Beijing Institute of Technology, Zhuhai, Zhuhai 519085, China.

* Corresponding authors.

E-mail addresses: shidaxin@bit.edu.cn (D. Shi), hanshengli@bit.edu.cn (H. Li)

Graphical Abstract



Highlights

- Mo species significantly promoted the hydrogenation of DCPD and inhibited the decomposition of DCPD.
- The aggregation of metallic Ni was restrained by Mo species.
- The adsorption modes of DCPD on catalyst surface changed with the introduction of Mo

Abstract

Mo promoted Ni/ γ -Al₂O₃ catalysts were synthesized by an incipient wetness co-impregnation method. The micro-structure, surface composition and adsorption characteristics of these catalysts were investigated by N₂ adsorption-desorption isotherms, XRD, HRTEM, XPS, TPR and dicyclopentadiene-TPD. The hydrogenation of dicyclopentadiene (DCPD) to endo-tetrahydrodicyclopentadiene (endo-THDCPD) was selected to evaluate the catalytic performance. The results showed Mo species improved dispersity of nickel oxide on the support surface and inhibit formation of spinel NiAl₂O₄. The nickel oxide could be reduced to Ni nanoparticles at relatively lower temperature because of its excellent dispersity and weakened interaction with the support. Meanwhile, the aggregation of metallic Ni on catalysts were markedly inhibited with the increasing of Mo content. Mo species also changed the adsorption mode of DCPD on Ni-based catalysts, and hence improved DCPD adsorption strength and capacity on catalysts and further changed hydrogenation mechanism of DCPD. The catalytic properties of NiMo_x/ γ -Al₂O₃ catalysts showed that the hydrogenation activity was increased by adding Mo to Ni-based catalyst within limits. When the ratio of Mo to Ni was 0.2, the NiMo_{0.2}/ γ -Al₂O₃ catalyst displayed the highest activity (TOF = 134.2 h⁻¹) and the best selectivity (99.7%). Compared with Ni/ γ -Al₂O₃ catalyst, the hydrogenation time reduced from 6 h to 3 h and the amount of by-product C₅ fraction significantly decreased from 2.4% to 0.3%.

Keywords: Dicyclopentadiene; Hydrogenation; Ni-Mo bimetallic catalyst; Adsorption mode

1. Introduction

Endo-tetrahydrodicyclopentadiene (endo-THDCPD) is not only a high-energy-density solid fuel [1] but also an important intermediate for the synthesis of adamantane [2-4] and exo-tetrahydrodicyclopentadiene (exo-THDCPD) [5-9]. The synthesis of endo-THDCPD has been attracting much attention in recent years. Generally, endo-THDCPD was synthesized by the hydrogenation of dicyclopentadiene (DCPD) [10,11] which was separated from the C₅ by-product of naphtha pyrolysis process [12,13]. There are two unsaturated double bonds in the chemical structure of DCPD, one is the double bond in norbornene ring (NB-bond) and the other is the double bond in cyclopentene ring (CP-bond). DFT simulation demonstrate the NB-bond strength is weaker than that of the CP-bond. Hence, in the hydrogenation process, NB-bond is saturated more easily than CP-bond. As a result, the majority of the hydrogenation intermediate is 8,9-dihydrodicyclopentadiene (8,9-DHDCPD) [14] (Scheme 1A). Another aspect has to be mentioned that DCPD can be decomposed to CPD in higher temperature [15,16]. The decomposition reaction (Scheme 1B) is the main reason for the reduction of the selectivity of endo-THDCPD in the hydrogenation of DCPD [16,17].

In previous works, Pd-based and Ni-based catalysts have been investigated for the hydrogenation of DCPD. Pd-based catalysts always show a high catalytic activity and selectivity with low reaction temperature. Pd/Al₂O₃ catalyst shows high activity for the hydrogenation of DCPD at low temperatures (90 °C) [10,11]. Pd/C catalyst also shows a good performance in the DCPD hydrogenation reaction, with the yield of endo-THDCPD reaching 97% in 30 min at 60 °C [18]. Nevertheless, due to the weak interaction between the metallic Pd and the support, the active centers of the Pd-based catalysts are easily sintered or lost during hydrogenation process. Furthermore, the Pd-based catalysts are susceptible to be poisoned by sulfide groups [19,20]. Besides, the high cost and rarity of Pd also limit its application in industry. Therefore, Ni-based catalysts as a substitute have been attracting lots

of researcher's interests in DCPD hydrogenation field.

Raney Ni is the only commercial hydrogenation catalyst in endo-THDCPD industry because of its low cost and high catalytic performance [21]. However, it suffers from inferior mechanical strength, poor reusability and complicated post-treatment procedure [22]. Therefore, it is necessary to find a suitable catalyst to replace Raney Ni. Zou et al. [14] investigated the hydrogenation of DCPD over SRNA-4 catalyst which was a kind of amorphous alloy Ni. The results showed that SRNA-4 exhibited significantly higher activity than Raney Ni under relatively mild conditions and the two-stage heating operation was more suitable to avoid the decomposition of DCPD. Wang et al. [22] prepared a kind of supported skeletal Ni catalyst that displayed better compressive strength than Raney Ni and good stability in the fixed-bed reactor. The above two catalysts were a kind of bulk Ni-based catalyst, which all had the problems of low activity and selectivity. The supported Ni-based catalyst can solve these problems because of great stability, low cost and high dispersion. Mi et al. [23] and Du et al. [24] prepared two kinds of Ni/ γ -Al₂O₃ catalysts with 15% and 30% Ni content and obtained the yield of endo-THDCPD reaching 95% and 93%, respectively. Sun et al. [21] prepared Ni-based catalysts using HY and α -Al₂O₃ as supports and the results showed that the mesoporous structure of α -Al₂O₃ could promote catalytic hydrogenation reaction because of sufficient contact of Ni atoms and DCPD molecules. Although supported Ni-based catalyst had unique advantages, the process of the DCPD hydrogenation should be carried out at high temperature in order to improve catalytic activity, which led to the tendency of DCPD decomposition and a bad endo-THDCPD selectivity. So, it is necessary to develop a highly active Ni-based catalyst to speed up the hydrogenation process and inhibit the decomposition of DCPD.

Ni-Mo bimetallic catalysts as a kind of hydrogenation catalysts are often used in the hydrogenation of unsaturated bonds [25-29]. In most of the bimetallic catalysts, Mo always acts as a promoter to modify the catalytic activity. The bimetallic Ni-Mo catalysts always show a higher hydrogenation activity than single metal Ni catalysts because the addition of Mo can improve the dispersion of Ni and effectively inhibit the strong interaction between

Ni and support, increase the hydrogen storage active site of Ni and change the outer layer valence electron structure of Ni, modify the activity and selectivity of the catalyst [30-32]. To the extent of our good knowledge, using NiMo/ γ -Al₂O₃ as a catalyst for the hydrogenation of DCPD and inhibiting the thermal decomposition of DCPD have not yet been reported.

In this work, a series of the NiMo/ γ -Al₂O₃ bimetallic catalysts were synthesized by using an incipient wetness co-impregnation method. The structure, physicochemical properties, and catalytic performance of these catalysts were investigated. Probing the synergistic Mo/Ni molar ratio of NiMo_x/ γ -Al₂O₃ bimetallic catalysts for the hydrogenation of DCPD and investigating the influence of Mo on the chemistry, structure and catalytic activity of NiMo_x/ γ -Al₂O₃ are the main purpose of the present work.

2. Experimental section

2.1. Materials

Ni(NO₃)₂·6H₂O (Sinopharm Chemical Reagent Co., Ltd), (NH₄)₆Mo₇O₂₄·4H₂O (Alfa Aesar) and γ -Al₂O₃ (Shandong Ruiding Technology Co., Ltd.) were used as purchased. γ -Al₂O₃ was dried for 6 h at 120 °C before use.

2.2. Preparation and activation of catalysts

The preparation of NiMo/ γ -Al₂O₃ catalysts was achieved by incipient wetness co-impregnation of γ -Al₂O₃ with mixed aqueous solution of Ni(NO₃)₂·6H₂O and (NH₄)₆Mo₇O₂₄·4H₂O. The impregnated sample was dried at 120 °C overnight, followed by calcination in air at 350 °C for 3 h. Before the hydrogenation, the precursor was activated by reduction in a horizontal quartz tubular reaction chamber under atmospheric pressure at 500 °C for 3 h. The Ni mass content was fixed as 10wt.%, and Mo mass content was varied with the change of molar ratios Mo/Ni at 0, 0.02, 0.05, 0.1, 0.2 and 0.5. The prepared catalysts

were labeled as Ni/ γ -Al₂O₃, NiMo_{0.02}/ γ -Al₂O₃, NiMo_{0.05}/ γ -Al₂O₃, NiMo_{0.1}/ γ -Al₂O₃, NiMo_{0.2}/ γ -Al₂O₃ and NiMo_{0.5}/ γ -Al₂O₃, respectively. And their precursors were denoted as NiO-MoO₃ *x*/ γ -Al₂O₃ (*X* = 0.02, 0.05, 0.1, 0.2 and 0.5) and NiO/ γ -Al₂O₃. Besides, single metal Mo sample (10wt.%, Mo/ γ -Al₂O₃) was prepared as control, and its precursor was assigned as MoO₃/ γ -Al₂O₃.

2.3. Characterization of catalyst and support

N₂ adsorption-desorption isotherms of catalysts were measured by using BELSORP-max to estimate the specific surface area and pore size distribution. The specific surface areas were estimated by using the Brunner-Emmet-Teller (BET) method, and the pore size distributions were calculated by the Barrett-Joyner-Halenda (BJH) method from the desorption isotherms. X-ray powder diffraction (XRD) was analyzed by a Philips X'Pert Pro Multipurpose X-ray diffractometer with Cu K α radiation. Temperature-programmed reduction (TPR) and DCPD temperature-programmed desorption (DCPD-TPD) were performed on a dynamic adsorption instrument (TP-5076) equipped with a thermal conductivity detector (TCD). In the TPR experiment, the sample (100 mg) was pretreated at 300 °C in Ar for 1 h and then cooled to room temperature. A gas mixture of H₂ (5%)/Ar (95%) was used as the reducing agent with a total flow rate of 50 mL/min. The samples were heated to 980 °C (10 °C/min) and the TPR profile was recorded simultaneously. For DCPD-TPD, firstly, precursors had been reduced in-situ at 500 °C (10 °C/min) in H₂ (5%)/He (95%) for 1 h, and the adsorption of DCPD over the catalyst was controlled at 30 °C for 30 min. After that the sample was purged with He for 1 h and then DCPD-TPD was performed in the range of 30-650 °C (10 °C/min). The desorbed DCPD was detected by TCD. The transmission electron microscopy (TEM), high-resolution TEM (HRTEM), high angle annular dark field-scanning transmission electron microscopy (HAADF-STEM) and EDS-elemental mapping tests were performed on a JEOL JEM-2100F system operated at 300 kV. X-ray photoelectron spectroscopy (XPS) spectra were recorded using a Thermo ESCALAB

250XI. Binding energy was calibrated using adventitious carbon at 284.8eV.

2.4. Catalytic testing

The hydrogenation of DCPD was carried out in a 100 ml stainless steel autoclave (Shanghai laibei Scientific Instruments Co., Ltd.) equipped with a mechanical agitator, a pressure controller and a temperature controller. Cyclohexane was selected as the reaction solvent. Prior to the reaction, 0.5 g pre-reduced catalyst, 5 g DCPD and 50 g cyclohexane were introduced in the reactor vessel. The reaction conditions were set at 150 °C, 3.5 MPa and a stirring rate of 600 rpm. A back-pressure valve was used to guarantee constant pressure in the autoclave. Liquid samples of 1 ml were taken from the reactor every hour and analyzed. The quantitative analysis of liquid mixtures was analyzed by a gas chromatograph (GC-2014, SHIMADZU, Japan) equipped with a HP-5MS column (30 m × 0.25 mm × 0.25 μm) and a flame ionization detector (FID). The area normalization method was used to quantitatively analyze the conversion of DCPD and the yield of each product. The turnover frequency (TOF) of the hydrogenation of DCPD on the catalytic sites (Ni) of the catalysts were calculated by dividing the number of DCPD converted per hour by the number of exposed Ni atoms on the surface of the catalysts determined by XPS.

3. Results and discussion

3.1. Structures of NiMo_x/γ-Al₂O₃ catalysts

N₂ adsorption-desorption isotherms and the pore size distributions of the oxide precursors were shown in Fig. 1. From Fig. 1a, all precursors and γ-Al₂O₃ support exhibited similar type-IV N₂ adsorption-desorption isotherms, which had typical H2 shape hysteresis loops at P/P₀ = 0.6-1.0 [33,34]. This denoted that Mo and Ni oxides did not change the mesoporous structure of γ-Al₂O₃ support [35]. A single peak distribution centered at about 7-8 nm was observed in all cases (Fig. 1b). This was in line with the relatively high specific

surface areas and the small mean pore diameters determined for all samples (Table 1).

As shown in Table 1, All oxide precursors showed the same structural characteristics as γ -Al₂O₃, such as high surface area (198-236 m²/g), relative large pore volume (0.46-0.64 cm³/g) and mean pore diameter (9.2-10.8 nm). With the increase of the Mo loading, the surface area and the pore size presented a subtle decrease. This indicated that the pores were not obviously blocked by the active components and the supported species were well dispersed on the γ -Al₂O₃ support [36]. And this result was also proved by XRD patterns.

Fig. 2a illustrated the XRD patterns of catalyst precursors and the support γ -Al₂O₃. Three main peaks at 2θ equaled to 37.60°, 45.79° and 66.76° revealed the presence of γ -Al₂O₃ phase (JCPDS 29-0063) in all samples. No diffraction peaks derived from NiO, MoO₃ or other phases such as NiMoO₄ and NiAl₂O₄ detected in NiO-MoO₃_x/ γ -Al₂O₃ (X = 0.02, 0.05, 0.1, 0.2 and 0.5) and NiO/ γ -Al₂O₃ precursors, which meant that the precursors maintain the base structure of γ -Al₂O₃ and the oxides of Ni and Mo uniformly dispersed on the surface of support without obvious agglomeration [35,37-39] and the same conclusion was also drawn from the characterization of N₂ adsorption-desorption isotherms.

Fig. 2b illustrated the XRD patterns of NiMo_x/ γ -Al₂O₃ (X = 0.02, 0.05, 0.1, 0.2 and 0.5) and Ni/ γ -Al₂O₃ catalysts. Besides the broad peak of γ -Al₂O₃, a relatively narrow diffraction peak at 51.85° (JCPDS 04-0850) corresponding to the metallic Ni was shown in the XRD pattern of the Ni/ γ -Al₂O₃ catalysts. It meant that the aggregation of metallic Ni occurred during the high temperature reduction process which led to the larger Ni particles appeared on the surface of the γ -Al₂O₃ support. Comparing with diffraction peak of Ni/ γ -Al₂O₃, the peak of NiMo_x/ γ -Al₂O₃ (X = 0.02, 0.05, 0.1, 0.2 and 0.5) at 51.85° became broader and its intensity became lower regularly with the increase of Mo loading until no obvious Ni diffraction peaks appeared in the XRD patterns of NiMo_{0.2}/ γ -Al₂O₃. This led to the conclusion that the average particle size of Ni was decreasing [26], which indicated that the aggregation of metallic Ni could be restrained by adding Mo species [40,41] and this effect gradually strengthened with the rise of Mo loading. However, when the content of Mo was further increased, the patterns were almost the same in both NiMo_{0.5}/ γ -Al₂O₃ and NiMo_{0.2}/ γ -

Al₂O₃. It illustrated that the inhibitory effect of Mo could be optimal when the ratio of Mo/Ni reached 0.2.

The TEM images visualized much better that NiMo_{0.2}/γ-Al₂O₃ (Fig. 3 B1) showed a better dispersion of metal particles compared with Ni/γ-Al₂O₃ (Fig. 3 A1). The HRTEM images of Ni/γ-Al₂O₃ and NiMo_{0.2}/γ-Al₂O₃ catalysts were given in Fig. 3 A2 and B2. As can be seen, the dark black near-spherical shaped Ni particles were located on the surface of γ-Al₂O₃ support (gray color, no obvious lattice fringe) and the crystal planes of the (111) of metallic nickel (about 0.203 nm) were clearly observed. Compared to Ni/γ-Al₂O₃, it could be clearly observed from NiMo_{0.2}/γ-Al₂O₃ that the size of Ni particles significantly decreased. It meant that Mo species were able to inhibit the sintering process of Ni particles and improved the dispersity of metallic Ni [42,43]. More HRTEM micrographs of NiMo_X/γ-Al₂O₃ (X = 0.02, 0.05, 0.1, and 0.5) catalysts were given in the supporting information (Fig. S1). Seen from these pictures, the size of Ni particles decreased gradually with increasing of Mo content which was well consistent with the XRD results of the reduced catalysts (Fig. 2b). HAADF-STEM and EDS-elemental mapping tests for the all catalysts were performed to further investigate the elemental distributions. As can be seen in Fig. S2, all the supported elements (Ni and Mo) were distributed homogeneously on the γ-Al₂O₃ which was also confirmed the conclusion drawn from TEM.

3.2. Reducibility of NiMo_X/γ-Al₂O₃ catalysts

The reducibility of the supported oxide species and their interaction with γ-Al₂O₃ support were studied by TPR. Fig. 4a illustrated the TPR profiles of MoO₃/γ-Al₂O₃, NiO/γ-Al₂O₃ and NiO-MoO₃_X/γ-Al₂O₃ (X = 0.02, 0.05, 0.1, 0.2 and 0.5). The TPR curve of MoO₃/γ-Al₂O₃ had two hydrogen consumption peaks centered at 475 °C and 878 °C [37,44]. The former could be assigned to the reduction of Mo⁶⁺ → Mo⁴⁺, and the latter was attributed to the further reduction of Mo⁴⁺ → Mo⁰. The TPR profile of NiO/γ-Al₂O₃ catalyst presented a distinct H₂ consumption peak centered at 524 °C and a broad peak at about 754 °C. As shown

in Fig. 4b, the first, strong, peak at the range of 350-550 °C could be deconvoluted into two NiO species [26]. The shoulder peak at low temperature was attributed to the reduction of loosely attached NiO crystals with rather low dispersion. The main peak arose from well dispersed NiO exhibiting moderate interaction with support surface. The second, minor, broad band was assigned to the reduction of NiAl₂O₄, which was strongly bonded to the support and hard to be reduced [40]. The peak area of 524 °C was several times larger than that of 754 °C that meant the content of NiO was much more than NiAl₂O₄. The TPR profiles of NiO-MoO₃_x/γ-Al₂O₃ (X = 0.02, 0.05, 0.1, 0.2 and 0.5) were more similar to NiO/γ-Al₂O₃ rather than MoO₃/γ-Al₂O₃ for the reason that the content of Mo species was low. Compared NiO-MoO₃_x/γ-Al₂O₃ (X = 0.02, 0.05, 0.1, 0.2 and 0.5) with NiO/γ-Al₂O₃, there were two interesting phenomena. Firstly, with the increasing of Mo content, the relative content of well dispersed NiO increased significantly. More details were given in the supporting information (Fig. S3 & Table S1). Secondly, the centered temperatures of the first H₂ consumption peaks gradually shifted to the low temperature range (508°C → 480°C) (Fig. 4a). An explanation was proposed for these phenomena that the incorporation of Mo species promoted the dispersion of NiO and decreased their particle size [41], and hence increased the reducibility of NiO over these five catalysts. As mentioned earlier, the reduction of Mo-oxo species had two main H₂ consumption peaks at around 475 °C and 878 °C, and the latter peak area was larger than that of the former peak. So the reduction of NiAl₂O₄ and the further reduction of Mo-oxo species from Mo⁴⁺ to Mo⁰ were the two main effects on the second peak (T_{R2}) of NiO-MoO₃_x/γ-Al₂O₃ (X = 0.02, 0.05, 0.1, 0.2 and 0.5) TPR profiles. Owing to the existence of Mo species, the T_{R2} peak area of NiO-MoO₃_x/γ-Al₂O₃ (X = 0.02, 0.05, 0.1, 0.2 and 0.5) increased with the rise of Mo content. Moreover, an obvious down-shift of T_{R2} peaks, compared with 878 °C, occurred due to the catalysis of metallic Ni. The variation content of NiAl₂O₄ on the surface of NiO-MoO₃_x/γ-Al₂O₃ (X = 0.02, 0.05, 0.1, 0.2 and 0.5) could not be obtained from this pattern, and this was going to be investigated by the XPS.

To attain further insight into the atomic ratios and chemical state of surface metals in all catalysts, XPS measurements were carried out for the NiMo_x/γ-Al₂O₃ (X = 0.02, 0.05, 0.1,

0.2 and 0.5) and Ni/ γ -Al₂O₃ catalysts. The average atomic composition on the surface of the samples were obtained from the total peak area and relative correction factors of Ni2p_{3/2} and Mo3d photoelectrons. As shown in Table 2, the percentage composition of Ni was basically stable at 2.2-2.4%, and the calculated values of Ni/Mo atomic ratio were in line with the actual values in catalysts preparation. Due to the low content of Mo, Mo was not detected on the surface of NiMo_{0.02}/ γ -Al₂O₃ catalyst.

The experimental and fitted Ni2p_{3/2} spectra peaks of the six Mo-Ni bimetallic catalysts were shown in Fig. 5. The XPS pattern of Ni2p_{3/2} could be deconvoluted into three chemical species (Ni⁰, NiO and NiAl₂O₄). Three peaks centered at 853.1 ± 0.1 eV, 855.9 ± 0.1 eV and 856.9 ± 0.1 eV were assigned to Ni⁰, NiO and NiAl₂O₄, respectively [36]. Moreover, from the total peak area of Ni and three kind of Ni species, the molar ratios of Ni⁰/Ni, NiO/Ni and NiAl₂O₄/Ni had been obtained. The above parameters were present in Table 2. It could be seen that most of Ni element existed in the form of nickel oxide and only a portion of nickel oxide was reduced to zero-valent state. This corresponded to the pattern of TPR that only a part of NiO could be reduced to metallic Ni at 500°C. Moreover, the molar ratio of Ni⁰/Ni varied from 0.16 (Ni/ γ -Al₂O₃) to 0.28 (NiMo_{0.2}/ γ -Al₂O₃), with the increasing of Mo content. This demonstrated that the reducibility of NiO was improved by the co-existence of Mo species. However, NiMo_{0.5}/ γ -Al₂O₃ and NiMo_{0.2}/ γ -Al₂O₃ exhibited almost the same proportion of Ni species. This conclusion conformed with the result that drawn from XRD that the optimal additive proportion of Mo was 0.2. Furthermore, it could also be seen that the molar ratio of NiAl₂O₄/Ni decreased with increasing of Mo loading. The possible reasons were that the well dispersed Mo species weakened the nickel species-support interactions, and thus inhibited the formation of spinel NiAl₂O₄ during the catalyst preparation. Thence, a conclusion could be drawn that the presence of Mo improved the dispersion and reduction of NiO and decreased the formation of NiAl₂O₄.

Fig. 6 showed the Mo3d XPS patterns of NiMo_X/ γ -Al₂O₃ (X = 0.1, 0.2 and 0.5) catalysts. Three doublets Mo3d_{5/2}-Mo3d_{3/2} corresponded, respectively, to the three valence states of Mo. The binding energies at 229.3 ± 0.1 eV and 231.6 ± 0.1 eV were ascribed to the

3d_{5/2} and 3d_{3/2} levels of Mo⁰ [31], while 232.0 ± 0.1 eV and 234.3 ± 0.1 eV associated with Mo⁴⁺ species of the MoO₂ phase [46], and finally 232.9 ± 0.1 eV and 235.4 ± 0.1 eV related to Mo⁶⁺ in unreduced MoO₃ [46,47]. From the Table 2, it should be noted that the catalysis of metallic nickel promoted the reduction of Mo⁴⁺ to Mo⁰ at a relatively low temperature, so there was a portion of Mo phase on the catalyst surfaces. Along with the Mo content increasing, the ratio of Mo⁰/Mo increased. Moreover, the proportion of Mo⁴⁺ showed a significant difference between these three catalysts, that it reached the maximal value in NiMo_{0.2}/γ-Al₂O₃ catalyst. This was in line with the result of DCPD-TPD. Finally, it could be seen that most of Mo element existed in the form of MoO₃ phase without being reduced. Hence, a conclusion could be drawn that the relative contribution of these three valence states could be adjusted by altering the molar ratio Mo/Ni in catalyst. The relevance between the DCPD-TPD characterization results and the ratio of Mo⁴⁺/Mo allowed us to make a conjecture about the role of Mo in the hydrogenation process.

3.3. Adsorption-desorption properties of NiMo_x/γ-Al₂O₃ catalysts

A large number of literatures have shown that the unsaturated carbon-carbon double bond has two adsorption states on the metal catalyst surface [48-50]. One is weakly adsorption of double bond with π-bond site, the other is strongly adsorption with di-σ-bond site. Therefore, there were eight possible adsorption states of DCPD on the surface of Ni-Mo bimetallic catalysts (Scheme 2). Scheme 2 (C-3) adsorption mode was hard to be formed due to the non-parallel structure of two unsaturated bond. Scheme 2 (A-2) and Scheme 2 (C-2) were also rare on the surface of catalyst due to the NB-bond strength was weaker than the CP-bond [14].

To investigate the adsorption-desorption properties of DCPD on samples, DCPD-TPD measurements were carried out for the NiMo_x/γ-Al₂O₃ (X = 0.02, 0.05, 0.1, 0.2 and 0.5), Ni/γ-Al₂O₃, Mo/γ-Al₂O₃ catalysts and γ-Al₂O₃ support (Fig. 7). As far as DCPD-TPD results were concerned, γ-Al₂O₃ and Mo/γ-Al₂O₃ both only had one distinct low temperature

desorption peak illustrating that the adsorption strength of DCPD on γ -Al₂O₃ or Mo/ γ -Al₂O₃ was weak. For γ -Al₂O₃, the peak derived from the desorption of DCPD on the Lewis acid sites of γ -Al₂O₃. For Mo/ γ -Al₂O₃, the peak area was larger than that from γ -Al₂O₃, indicating the adsorption of DCPD occurred on Mo species (Mo⁴⁺). And this adsorption strength was stronger than that of γ -Al₂O₃ due to the up-shift of the peak. However, two peaks (T_{d1} and T_{d2}) were observed from Ni/ γ -Al₂O₃ catalyst implying that the DCPD had two adsorption states on the Ni/ γ -Al₂O₃ catalyst with different strength. The aforementioned statement that T_{d1} at relatively low temperature (113 °C) was ascribed to weakly π -bonded DCPD desorbed from metallic Ni (Scheme 2B), and T_{d2} at relatively high temperature (309 °C) corresponded to the desorption of di- σ -bonded DCPD species (Scheme 2A). By comparing Ni/ γ -Al₂O₃ with Mo/ γ -Al₂O₃, it could be concluded that Ni was the active site to form strongly di- σ -bonded adsorption, which was the main active adsorption of DCPD.

More interestingly, in the profiles of the four Mo-Ni bimetallic catalysts NiMo_x/ γ -Al₂O₃ (X = 0.02, 0.05, 0.1 and 0.2), with the increasing of Mo/Ni ratio to 0.2, firstly, the peak area for both low and high temperature desorption peak area increased simultaneously, indicating that the addition of Mo element raised the DCPD adsorption capacity of catalysts. And the improving dispersion of metallic Ni was the main reason for the increase of the high temperature peak area. Secondly, the second desorption peak of DCPD gradually shifted to the higher temperature, demonstrating that Mo promoter enhanced the adsorption strength of DCPD over bimetallic catalyst. The possible reason was that the addition of Mo species increased the amount of mixed-pin adsorption mode (Scheme 2 (C-1)), in which NB-band adsorbed on metallic Ni with di- σ -bond form and CP-band adsorbed on Mo species (Mo⁴⁺) with π -bond form. However, things were different when the ratio of Mo/Ni increased to 0.5. there was no significant increase or shifting in the peak area and temperature of NiMo_{0.5}/ γ -Al₂O₃, compared with NiMo_{0.2}/ γ -Al₂O₃. This was in line with the result of XPS (Table 2, column 9) that the value of Mo⁴⁺/ Mo reached the summit at NiMo_{0.2}/ γ -Al₂O₃. It further illustrated that the optimal ratio of Mo/Ni was located at 0.2. As testified by the catalysts evaluation, the increasing of DCPD adsorption capacity and strength was beneficial to the

hydrogenation reaction of DCPD.

3.4. Catalysts evaluation

Fig. 8a showed the DCPD conversion rate using any one of Ni/ γ -Al₂O₃, NiMo_X/ γ -Al₂O₃ (X = 0.02, 0.05, 0.1, 0.2 and 0.5) and Mo/ γ -Al₂O₃ catalysts. The DCPD could achieve complete conversion within 6 h over all catalysts, except for Mo/ γ -Al₂O₃. It took 4 h to reach 97% conversion of DCPD on Ni/ γ -Al₂O₃ and NiMo_{0.02}/ γ -Al₂O₃ catalysts. With the further increasing of Mo content, the conversion rate of DCPC was gradually accelerating. Conversion speed of DCPD on NiMo_{0.2}/ γ -Al₂O₃ was two times faster than Ni/ γ -Al₂O₃ or NiMo_{0.02}/ γ -Al₂O₃ catalysts. Only in 2 h the conversion of DCPD reached 97% under NiMo_{0.2}/ γ -Al₂O₃. This clearly indicated that Mo was promoting the hydrogenation of DCPD on Ni-based catalysts. However, things were different as more Mo added to 0.5. The conversion rate had a slight decline compared with that over NiMo_{0.2}/ γ -Al₂O₃.

Fig. 8b showed the yield of intermediate 8,9-DHDCPD under different catalysts. Apart from Mo/ γ -Al₂O₃, the content of 8,9-DHDCPD firstly increased and then decreased, but the generation and conversion rate of 8,9-DHDCPD were markedly different. For Ni/ γ -Al₂O₃ and NiMo_{0.02}/ γ -Al₂O₃, it took approximate 2 h, the contents of 8,9-DHDCPD reached the maximum value and then gradually decreased. However, for NiMo_X/ γ -Al₂O₃ (X = 0.05, 0.1, 0.2 and 0.5), it took only 1 h to reach the peak. This illustrated the generation and conversion rate of 8,9-DHDCPD could be enhanced by adding Mo to Ni-based catalyst within limits. Another interesting phenomenon was that the maximum content of intermediate 8,9-DHDCPD in the reaction system decreased with the ratio of Mo increasing from 0.05 to 0.2. The decreased of the maximum intermediate content meant that the reaction rate ratio of the second hydrogenation step to the first hydrogenation step raised.

Fig. 8c showed the curves of the yield of product endo-THDCPD. Adding Mo accelerated the producing of endo-THDCPD. When the amount of Mo (Mo/Ni=0.02) was low, there was no acceleration effect. And when the amounts of Mo (Mo/Ni=0.05, 0.1 and

0.2) were larger, the acceleration effect was obviously improved. Nevertheless, As the continuation of Mo content increased after loading over 0.2, the evaluation result of $\text{NiMo}_{0.5}/\gamma\text{-Al}_2\text{O}_3$ deviated from the above conclusion. Under the $\text{Mo}/\gamma\text{-Al}_2\text{O}_3$ catalyst, the product endo-THDCPD was almost undetected, which further illustrated that Ni was the main active component of this system.

Turnover frequency (TOF) reflected the intrinsic activity of the active sites (exposed surface Ni metal) in the catalyst, and the changes of TOF could be observed by adjusting Mo/Ni value (Fig. 9). The mass content of Ni was fixed at 10wt.% for all catalysts. However, with the increasing of Mo content, the TOF on Ni-based catalysts increased, and the optimum molar ratio of Mo/Ni was located at 0.2, with the TOF value of 134.2 h^{-1} , which was twice as that of $\text{Ni}/\gamma\text{-Al}_2\text{O}_3$ (TOF = 67.2 h^{-1}). When the content of Mo increased to 0.5, the catalytic activity of $\text{NiMo}_{0.5}/\gamma\text{-Al}_2\text{O}_3$ declined (TOF = 106.8 h^{-1}).

Three possible reasons could be applied to explain why the catalytic performance of $\text{NiMo}_X/\gamma\text{-Al}_2\text{O}_3$ ($X = 0.02, 0.05, 0.1$ and 0.2) were gradually enhanced. The first was that both the dispersity and the active surface area of Ni were increased with the addition of Mo content. Another reason was the increasing reducibility of NiO and the decrease of inactive nickel aluminate on the surface of the catalyst. Third, and perhaps most significant, was that both the adsorption capacity and the adsorption strength of DCPD on $\text{NiMo}_X/\gamma\text{-Al}_2\text{O}_3$ had increased (Fig. 7). It was generally known that hydrogenation of unsaturated double bond on the surface of heterogeneous catalyst needed at least three steps: adsorption, surface reaction and desorption. DCPD had two unsaturated double bonds (NB-bond and CP-bond). For $\text{Ni}/\gamma\text{-Al}_2\text{O}_3$ catalyst, most of adsorption DCPD species were in the form of Scheme 2 (A-1) that only NB-bond adsorbed on the surface of catalyst. There would be a process in which the 8,9-DHDCPD was desorbed from catalyst after the NB-bond was hydrogenated and then the 8,9-DHDCPD was adsorbed to catalyst again and hydrogenated the CP-bond (Scheme 3 A). This might be the reason why the hydrogenation rate was slow and the concentration of 8,9-DHDCPD was high for $\text{Ni}/\gamma\text{-Al}_2\text{O}_3$. Nevertheless, with the addition of Mo, the mixed-pin adsorption mode (Scheme 2 (C-1)) appeared. For this adsorption mode, a surface migration

of intermediate product happened when the NB-bond hydrogenation was finished. The adsorption site of 8,9-DHDCPD moved from Mo species (π -bond site) to adjacent metallic Ni (di- σ -bond site). This led to a possible hydrogenation pathway that a portion of the intermediate product continued to hydrogenate on the catalyst surface without undergoing a desorption process (Scheme 3B). With the increasing of Mo content from 0.02 to 0.2, the proportion of mixed-pin adsorption mode on the surface of catalyst was increased simultaneously, but a small part of mono-pin adsorption mode (Scheme 2 (A-1)) still existed in the surface of catalysts. This could explain why the hydrogenation rate of $\text{NiMo}_X/\gamma\text{-Al}_2\text{O}_3$ ($X = 0.02, 0.05, 0.1$ and 0.2) were sped up in turn and the concentration of 8,9-DHDCPD showed a decrease tendency. For $\text{NiMo}_{0.5}/\gamma\text{-Al}_2\text{O}_3$, the decreasing of specific surface area, pore size and the value of Mo^{4+}/Mo might be the reason for the decrease of catalyst activity.

It was also interesting that, with the increment of Mo content on Ni-based catalysts, the yield of by-product C_5 fraction (cyclopentadiene & cyclopentene & cyclopentane) showed a significantly decline trend (Fig. 8d). For $\text{Ni}/\gamma\text{-Al}_2\text{O}_3$, the final yield of C_5 fraction was about 2.4%. For the $\text{NiMo}_{0.2}/\gamma\text{-Al}_2\text{O}_3$, that figure was only 0.3%. This could be attributed to the enhanced DCPD adsorption strength on the $\text{NiMo}_{0.2}/\gamma\text{-Al}_2\text{O}_3$ catalyst surface, thus promoting the DCPD hydrogenation pathway (Scheme 1A). Therefore, one conclusion could be fairly drawn that the addition of Mo could effectively inhibit the decomposition of DCPD during the hydrogenation process. And this had a great significance for industrial production.

In summary, there were significant differences among the seven catalysts in the conversion rate of DCPD, the formation and consumption rate of 8,9-DHDCPD and its maximum yield, the production rate of endo-THDCPD and the yield of by-product. All these phenomena pointed to the conclusion that the addition of Mo species could not only increase the hydrogenation rate of Ni-based catalysts, inhibit the decomposition of DCPD, but also change the relative hydrogenation rate of CP-bond and NB-bond. However, the change in content of Ni and nickel aluminate could not affect or change the relative hydrogenation rate of CP-bond and NB-bond. So it might be that the change of the catalytic mechanism caused this phenomenon.

4. Conclusion

A series of Mo-promoted Ni/ γ -Al₂O₃ catalysts were synthesized by an incipient wetness co-impregnation method, and the supported species did not influence the structure of the support. The dispersion of NiO on precursors were promoted and the aggregation of metallic Ni on catalysts were restrained with increasing of Mo content. More catalytic active centers (Ni⁰) formed on the support due to the weakened strength of the nickel species-support interactions. Furthermore, the addition of Mo changed the adsorption mode of DCPD on catalyst surface, which had a significant effect on the performance of the catalysts. The catalytic properties of NiMo_X/ γ -Al₂O₃ (X = 0.02, 0.05, 0.1, 0.2 and 0.5) catalysts showed that in a certain range, the hydrogenation activity increased with the rise of Mo amount, and the optimal ratio of Mo/Ni was located at 0.2. The NiMo_{0.2}/ γ -Al₂O₃ catalyst displayed the highest activity (TOF=134.2 h⁻¹) and the best selectivity (99.7%). Compared with Ni/ γ -Al₂O₃ catalyst, the hydrogenation time reduced from 6 h to 3 h and the amount of by-product C₅ fraction significantly decreased from 2.4% to 0.3%.

Acknowledgements

We are very grateful to the National Natural Science Foundation of China (NNSFC) for the support (No.21576025).

Reference

- [1] C.A. Cohen, C.W. Muessig, US 3381046 A (1968).
- [2] M. Navrátilová, K. Sporka, *Appl. Catal. A: Gen.* 203 (2000) 127-132.
[https://doi.org/10.1016/S0926-860X\(00\)00477-4](https://doi.org/10.1016/S0926-860X(00)00477-4)
- [3] G.C. Lau, W.F. Maier, *Langmuir* 3 (1987) 164-173.
<https://doi.org/10.1021/la00074a004>
- [4] E.M. Engler, M. Farcasiu, A. Sevin, J.M. Cense, P.V. Schleyer, *J. Am. Chem. Soc.* 95 (1973) 5769-5771.
<https://doi.org/10.1021/ja00798a059>
- [5] E.H. Xing, Z.T. Mi, C.W. Xin, L. Wang, X.W. Zhang, *J. Mol. Catal. A: Chem.* 231 (2005) 161-167.
<https://doi.org/10.1016/j.molcata.2005.01.015>
- [6] C.M. Sun, G. Li, *Appl. Catal. A: Gen.* 402 (2011) 196-200.
<https://doi.org/10.1016/j.apcata.2011.06.008>
- [7] M.Y. Huang, J.C. Wu, *Fuel* 90 (2011) 1012-1017.
<https://doi.org/10.1016/j.fuel.2010.11.041>
- [8] H.S. Chung, C.S.H. Chen, R.A. Kremer, J.R. Boulton, G.W. Burdette, *Energy Fuels* 13 (1999) 641-649.
<https://doi.org/10.1021/ef980195k>
- [9] T. Edwards, *J. Propul. Power* 19 (2003) 1089-1107.
<https://doi.org/10.2514/2.6946>
- [10] G.Z. Liu, Z.T. Mi, L. Wang, X.W. Zhang, S.T. Zhang, *Ind. Eng. Chem. Res.* 45 (2006) 8807-8814.
<https://doi.org/10.1021/ie060660y>
- [11] G.Z. Liu, X.W. Zhang, L. Wang, S.T. Zhang, Z.T. Mi, *Chem. Eng. Sci.* 63 (2008) 4991-5002.
<https://doi.org/10.1016/j.ces.2008.03.008>
- [12] H. Han, J.J. Zou, X.W. Zhang, L.W. L. W, *Appl. Catal. A: Gen.* 367 (2009) 84-88.
<https://doi.org/10.1016/j.apcata.2009.07.035>
- [13] M.E. Jamróz, S. Gałka, J.C. Dobrowolski, *J. Mol. Struct.-Theochem* 634 (2003) 225-233.
[https://doi.org/10.1016/S0166-1280\(03\)00348-8](https://doi.org/10.1016/S0166-1280(03)00348-8)

- [14] JJ Zou, XW Zhang, J. Kong, L. Wang, *Fuel* 87 (2008) 3655-3659.
<https://doi.org/10.1016/j.fuel.2008.07.006>
- [15] H.J. Flammersheim, J. Opfermann, *Thermochim. Acta* 337 (1999) 149-153.
[https://doi.org/10.1016/S0040-6031\(99\)00163-X](https://doi.org/10.1016/S0040-6031(99)00163-X)
- [16] X.W. Zhang, L. Pan, L. Wang, J.J. Zou, *Chem. Eng. Sci.* 180 (2018) 95-125.
<https://doi.org/10.1016/j.ces.2017.11.044>
- [17] G.Z. Liu, Z.T. Mi, L. Wang, X.W. Zhang, *Ind. Eng. Chem. Res.* 44 (2005) 3846-3851.
<https://pubs.acs.org/doi/abs/10.1021/ie0487437>
- [18] M.L. Hao, B.L. Yang, H.G. Wang, G. Liu, S.T. Qi, *J. Phys. Chem. A* 114 (2010) 3811-3817.
<https://doi.org/10.1021/jp9060363>
- [19] N. Sadokhina, G. Smedler, U. Nylén, M. Olofsson, L. Olsson, *Appl. Catal. B: Environ.* 236 (2018) 384-395.
<https://doi.org/10.1016/j.apcatb.2018.05.018>
- [20] S. Yun, S. Lee, S. Yook, H.A. Patel, C.T. Yavuz, M. Choi, *ACS Catal.* 6 (2016) 2435-2442.
<https://doi.org/10.1021/acscatal.5b02613>
- [21] C.M. Sun, G. Li, *Acta Petrol. Sin.: Pet. Process. Sect.* 28 (2012) 296-302.
<https://doi.org/10.3969/j.issn.1001-8719.2012.02.021>
- [22] Y.L. Wang, G.H. Luo, X. Xu, J.J. Xia, *Catal. Commun.* 53 (2014) 15-20.
<https://doi.org/10.1016/j.catcom.2014.04.011>
- [23] Z.T. Mi, J. Yan, J.L. Li, Y. Xu, *J. Fuel Chem. Tech.* 25 (1997) 492-497.
- [24] Y.M. Du, C.Y. Li, L.G. Kou, Q. Xu, Q. Shi, J. Lu, *Spec. Petrochem.* 28 (2011) 21-24.
<https://doi.org/10.3969/j.issn.1003-9384.2011.02.006>
- [25] D. Kubička, L. Kaluža, *Appl. Catal. A: Gen.* 372 (2010) 199-208.
<https://doi.org/10.1016/j.apcata.2009.10.034>
- [26] E. Kordouli, B. Pawelec, K. Bourikas, C. Kordulis, J.L.G. Fierro, A. Lycourghiotis, *Appl. Catal. B: Environ.* 229 (2018) 139-154.
<https://doi.org/10.1016/j.apcatb.2018.02.015>
- [27] G. Escalonaa, A. Raia, P. Betancourt, A.K. Sinha, *Fuel* 219 (2018) 270-278.

<https://doi.org/10.1016/j.fuel.2018.01.134>

[28] S. Badoga, R.V. Sharma, A.K. Dalai, J. Adjaye, *Appl. Catal. A: Gen.* 489 (2015) 86-97.

<https://doi.org/10.1016/j.apcata.2014.10.008>

[29] G.W. Huber, P. O'Connor, A. Corma, *Appl. Catal. A: Gen.* 329 (2007) 120-129.

<https://doi.org/10.1016/j.apcata.2007.07.002>

[30] D.X. Zhang, J. Zhao, Y.Y. Zhang, X.L. Lu, *Int. J. Hydrogen Energy* 41 (2015) 11675-11681.

<https://doi.org/10.1016/j.ijhydene.2015.11.173>

[31] R.G. Kukushkin, O.A. Bulavchenko, V.V. Kaichev, V.A. Yakovlev, *Appl. Catal. B: Environ.* 163 (2015) 531-538.

<https://doi.org/10.1016/j.apcatb.2014.08.001>

[32] J.D. Xu, T.T. Huang, Y. Fan, *Appl. Catal. B: Environ.* 203 (2017) 839-850.

<https://doi.org/10.1016/j.apcatb.2016.10.078>

[33] F.R. Shamskar, M. Rezaei, F. Meshkani, *Int. J. Hydrogen Energy* 42 (2017) 4155-4164.

<https://doi.org/10.1016/j.ijhydene.2016.11.067>

[34] G. Leofantia, M. Padovan, G. Tozzola, B. Venturelli, *Catal. Today* 41 (1998) 207-219.

[https://doi.org/10.1016/S0920-5861\(98\)00050-9](https://doi.org/10.1016/S0920-5861(98)00050-9)

[35] W.G. Cui, W.H. Li, R. Gao, H.X. Ma, D. Li, M.L. Niu, X. Lei, *Energy Fuels* 31 (2017) 3768-3783.

<https://doi.org/10.1021/acs.energyfuels.6b03390>

[36] E. Kordouli, L. Sygellou, C. Kordulis, K. Bourikas, A. Lycourghiotis, *Appl. Catal. B: Environ.* 209 (2017) 12-22.

<https://doi.org/10.1016/j.apcatb.2017.02.045>

[37] K. Soni, B.S. Rana, A.K. Sinha, A. Bhaumik, M. Nandi, M. Kumar, G.M. Dhar, *Appl. Catal. B: Environ.* 90 (2009) 55-63.

<https://doi.org/10.1016/j.apcatb.2009.02.010>

[38] P.A. Nikulshin, P.P. Minaev, A.V. Mozhaev, K.I. Maslakov, M.S. Kulikova, A.A. Pimerzin, *Appl. Catal. B: Environ.* 176 (2015) 374-384.

<https://doi.org/10.1016/j.apcatb.2015.04.011>

[39] P. Rayo, A. Rodríguez-Hernández, P. Torres-Mancera, J.A.D. Muñoz, J. Ancheyta, R.G. de León,

Catal. Today 305 (2018) 2-12.

<https://doi.org/10.1016/j.cattod.2017.12.034>

[40] M.H. Youn, J.G. Seo, P. Kim, I.K. Song, J. Mol. Catal. A: Chem. 261 (2007) 276-281.

<https://doi.org/10.1016/j.molcata.2006.08.030>

[41] T. Borowiecki, W. Gac, A. Denis, Appl. Catal. A: Gen. 270 (2004) 27-36.

<https://doi.org/10.1016/j.apcata.2004.03.044>

[42] F.H. Meng, X. Li, M.H. Li, X.X. Cui, Z. Li, Chem. Eng. J. 313 (2017) 1548-1555.

<https://doi.org/10.1016/j.cej.2016.11.038>

[43] J. Newnham, K. Mantri, M.H. Amin, J. Tardio, S.K. Bhargava, Int. J. Hydrogen Energy 37 (2012) 1454-1464.

<https://doi.org/10.1016/j.ijhydene.2011.10.036>

[44] H. Liu, Y.P. Li, C.L. Yin, Y.L. Wu, Y.M. Chai, D.M. Dong, X.H. Li, C.G. Liu, Appl. Catal. B: Environ. 198 (2016) 493-507.

<https://doi.org/10.1016/j.apcatb.2016.06.004>

[45] S. Damyanova, B. Pawelec, K. Arishtirova, J.L.G. Fierro, Int. J. Hydrogen Energy 37 (2012) 15966-15975.

<https://doi.org/10.1016/j.ijhydene.2012.08.056>

[46] H. Chen, Q.F. Wang, X.W. Zhang, L. Wang, Fuel 159 (2015) 430-435.

<https://doi.org/10.1016/j.fuel.2015.07.010>

[47] W.K. Lai, W.J. Song, L.Q. Pang, Z.F. Wu, N. Zheng, J.J. Li, J.B. Zheng, X.D. Yi, W.P. Fang, J. Catal. 303 (2013) 80-91.

<https://doi.org/10.1016/j.jcat.2013.03.001>

[48] B. Zhu, B.W.L. Jang, J. Mol. Catal. A: Chem. 395 (2014) 137-144.

<https://doi.org/10.1016/j.molcata.2014.08.015>

[49] I.Y. Ahn, W.J. Kim, S.H. Moon, Appl. Catal. A: Gen. 308 (2006) 75-81.

<https://doi.org/10.1016/j.apcata.2006.04.027>

[50] Y.J. Chen, J.X. Chen, Appl. Surf. Sci. 387 (2016) 16-27. <https://doi.org/10.1016/j.apsusc.2016.06.067>

Table Captions

Table 1	Symbols and several characteristics of the precursors (specific pore volume (V_p), specific surface area (S_{BET}) and mean pore diameter (MPD)).
Table 2	Quantitative surface analysis of $NiMo_x/\gamma-Al_2O_3$ ($X = 0.02, 0.05, 0.1, 0.2$ and 0.5) and $Ni/\gamma-Al_2O_3$.

Scheme Captions

Scheme 1	Two reaction pathway during the hydrogenation of DCPD.
Scheme 2	Adsorption modes of DCPD on catalyst surface.
Scheme 3	Proposed hydrogenation mechanism of DCPD on the catalyst.

Figure Captions

Figure 1	N_2 adsorption-desorption isotherms (a) and pore size distributions (b) of the catalyst precursors $NiO-MoO_3_x/\gamma-Al_2O_3$ ($X = 0.02, 0.05, 0.1, 0.2$ and 0.5), $NiO/\gamma-Al_2O_3$ and $\gamma-Al_2O_3$.
Figure 2	XRD patterns of catalyst precursors $NiO-MoO_3_x/\gamma-Al_2O_3$ ($X = 0.02, 0.05, 0.1, 0.2$ and 0.5), $NiO/\gamma-Al_2O_3$ and $\gamma-Al_2O_3$ (a), fresh catalysts $NiMo_x/\gamma-Al_2O_3$ ($X = 0.02, 0.05, 0.1, 0.2$ and 0.5) and $Ni/\gamma-Al_2O_3$ (b).
Figure 3	HRTEM micrographs of $Ni/\gamma-Al_2O_3$ (A1-A2) and $NiMo_{0.2}/\gamma-Al_2O_3$ (B1-B2) catalysts.
Figure 4	TPR profiles of catalyst precursors $MoO_3/\gamma-Al_2O_3$, $NiO/\gamma-Al_2O_3$ and $NiO-MoO_3_x/\gamma-Al_2O_3$ ($X = 0.02, 0.05, 0.1, 0.2$ and 0.5) (a), deconvolution of the reduction curve of the $NiO/\gamma-Al_2O_3$ (b).
Figure 5	$Ni2p_{3/2}$ XPS patterns of $NiMo_x/\gamma-Al_2O_3$ ($X = 0.02, 0.05, 0.1, 0.2$ and 0.5) and $Ni/\gamma-Al_2O_3$.
Figure 6	$Mo3d$ XPS patterns of $NiMo_{0.1}/\gamma-Al_2O_3$ and $NiMo_{0.2}/\gamma-Al_2O_3$ and $NiMo_{0.5}/\gamma-Al_2O_3$.
Figure 7	DCPD-TPD profiles of $NiMo_x/\gamma-Al_2O_3$ ($X = 0.02, 0.05, 0.1, 0.2$ and 0.5),

Ni/ γ -Al₂O₃, Mo/ γ -Al₂O₃ catalysts and γ -Al₂O₃ support.

Figure 8 Conversion of DCPD (a), yield of 8,9-DHDCPD (b), yield of endo-THDCPD (c) and yield of C₅ fraction (d) varying with reaction time (mass ratio of catalyst to DCPD to cyclohexane is 1:10:100; temperature 150 °C; hydrogen pressure 3.5 MPa; stirring rate 600 rpm)

Figure 9 Turnover frequency (TOF, h⁻¹) of various Ni-based catalysts for hydrogenation of DCPD

ACCEPTED MANUSCRIPT

Table 1

Symbols and several characteristics of the precursors (specific pore volume (V_p), specific surface area (S_{BET}) and mean pore diameter (MPD)).

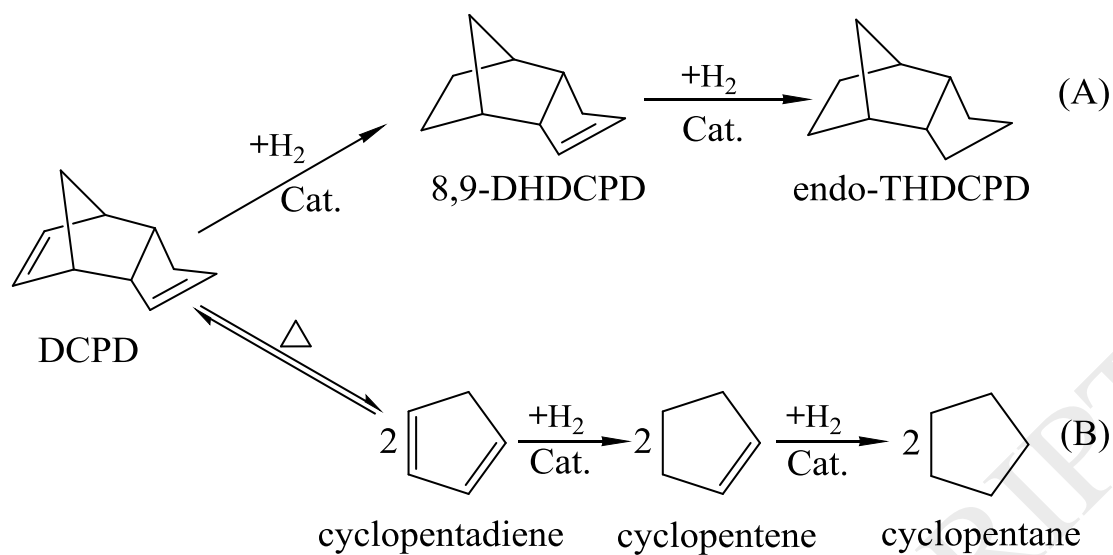
Sample	V_p (cm ³ /g)	S_{BET} (m ² /g)	MPD (nm)
γ -Al ₂ O ₃	0.64	236	10.8
NiO/ γ -Al ₂ O ₃	0.56	213	10.5
NiO-MoO ₃ 0.02/ γ -Al ₂ O ₃	0.54	213	10.2
NiO-MoO ₃ 0.05/ γ -Al ₂ O ₃	0.53	218	9.8
NiO-MoO ₃ 0.1/ γ -Al ₂ O ₃	0.49	201	9.7
NiO-MoO ₃ 0.2/ γ -Al ₂ O ₃	0.49	209	9.4
NiO-MoO ₃ 0.5/ γ -Al ₂ O ₃	0.46	198	9.2

Table 2

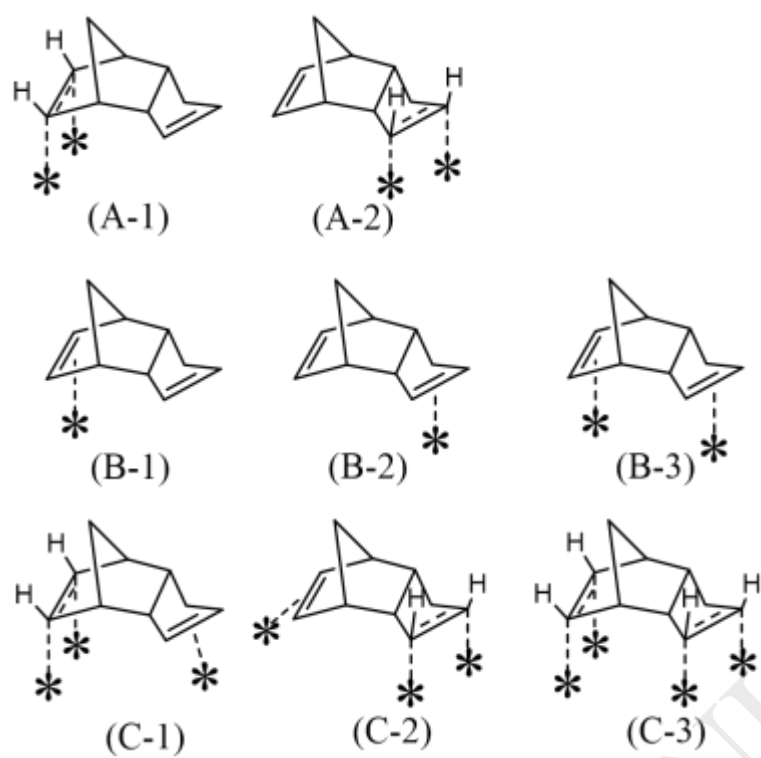
Quantitative surface analysis of NiMo_X/ γ -Al₂O₃ (X = 0.02, 0.05, 0.1, 0.2 and 0.5) and Ni/ γ -Al₂O₃.

Sample	SAC ^a (atomic %)		Ni/Mo	Ni ⁰ /Ni	NiO/Ni	NiAl ₂ O ₄ /Ni	Mo ⁰ /Mo	Mo ⁴⁺ /Mo	Mo ⁶⁺ /Mo
	Ni	Mo							
Ni/ γ -Al ₂ O ₃	2.4	–	–	0.16	0.68	0.16	–	–	–
NiMo _{0.02} / γ -Al ₂ O ₃	2.3	–	–	0.17	0.68	0.15	–	–	–
NiMo _{0.05} / γ -Al ₂ O ₃	2.2	0.1	0.04	0.21	0.66	0.13	–	–	–
NiMo _{0.1} / γ -Al ₂ O ₃	2.2	0.3	0.14	0.24	0.64	0.12	0.15	0.18	0.67
NiMo _{0.2} / γ -Al ₂ O ₃	2.2	0.5	0.23	0.28	0.63	0.09	0.18	0.28	0.54
NiMo _{0.5} / γ -Al ₂ O ₃	2.2	1.2	0.54	0.27	0.64	0.09	0.25	0.21	0.54

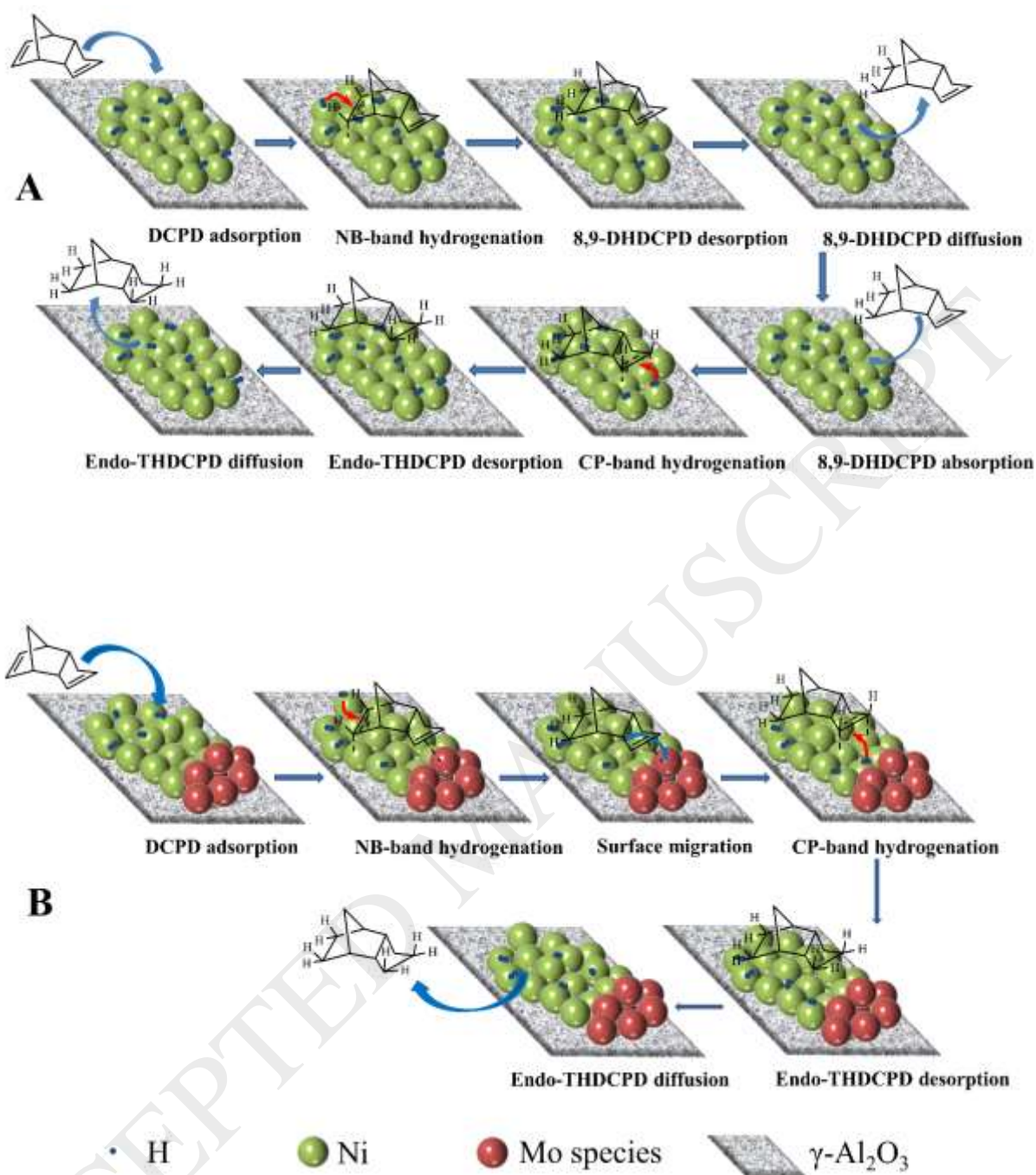
^a Surface atomic composition



Scheme 1. Two reaction pathway during the hydrogenation of DCPD.



Scheme 2. Adsorption modes of DCPD on catalyst surface.



Scheme 3. Proposed hydrogenation mechanism of DCPD on the catalyst.

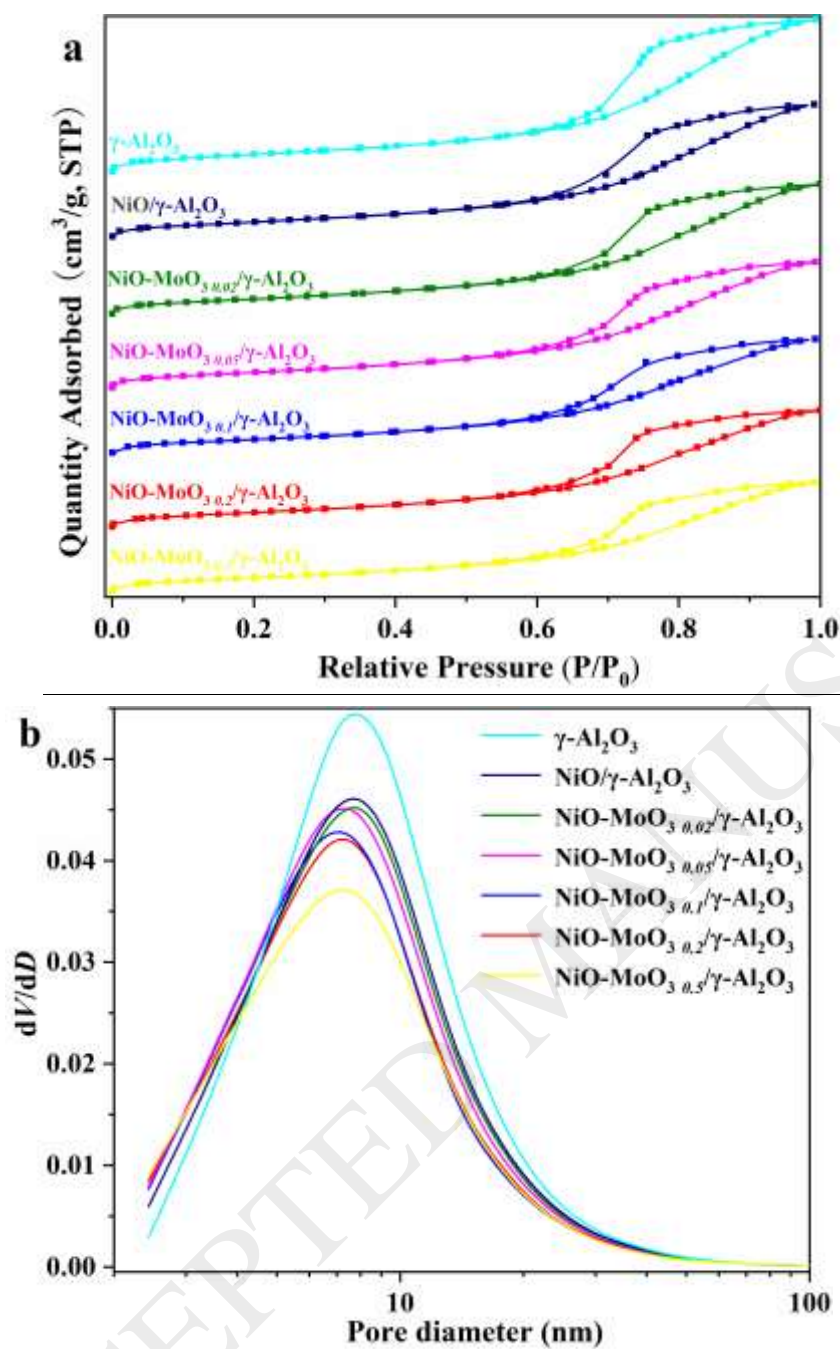


Fig. 1. N_2 adsorption-desorption isotherms (a) and pore size distributions (b) of the catalyst precursors $NiO-MoO_{3x}/\gamma-Al_2O_3$ ($X = 0.02, 0.05, 0.1, 0.2$ and 0.5), $NiO/\gamma-Al_2O_3$ and $\gamma-Al_2O_3$.

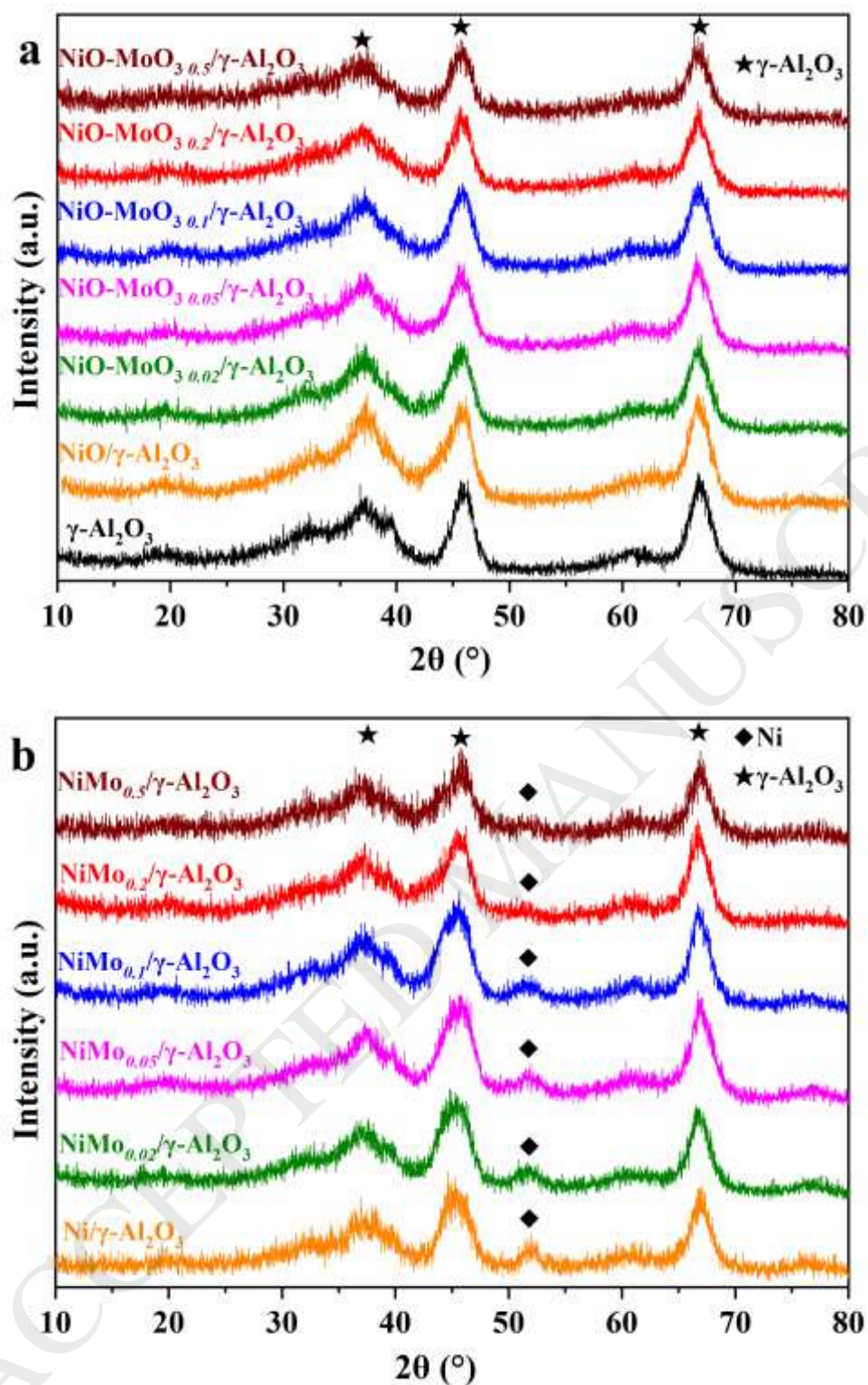


Fig. 2. XRD patterns of catalyst precursors $\text{NiO-MoO}_3_x/\gamma\text{-Al}_2\text{O}_3$ ($X = 0.02, 0.05, 0.1, 0.2$ and 0.5), $\text{NiO}/\gamma\text{-Al}_2\text{O}_3$ and $\gamma\text{-Al}_2\text{O}_3$ (a), fresh catalysts $\text{NiMo}_x/\gamma\text{-Al}_2\text{O}_3$ ($X = 0.02, 0.05, 0.1, 0.2$ and 0.5) and $\text{Ni}/\gamma\text{-Al}_2\text{O}_3$ (b).

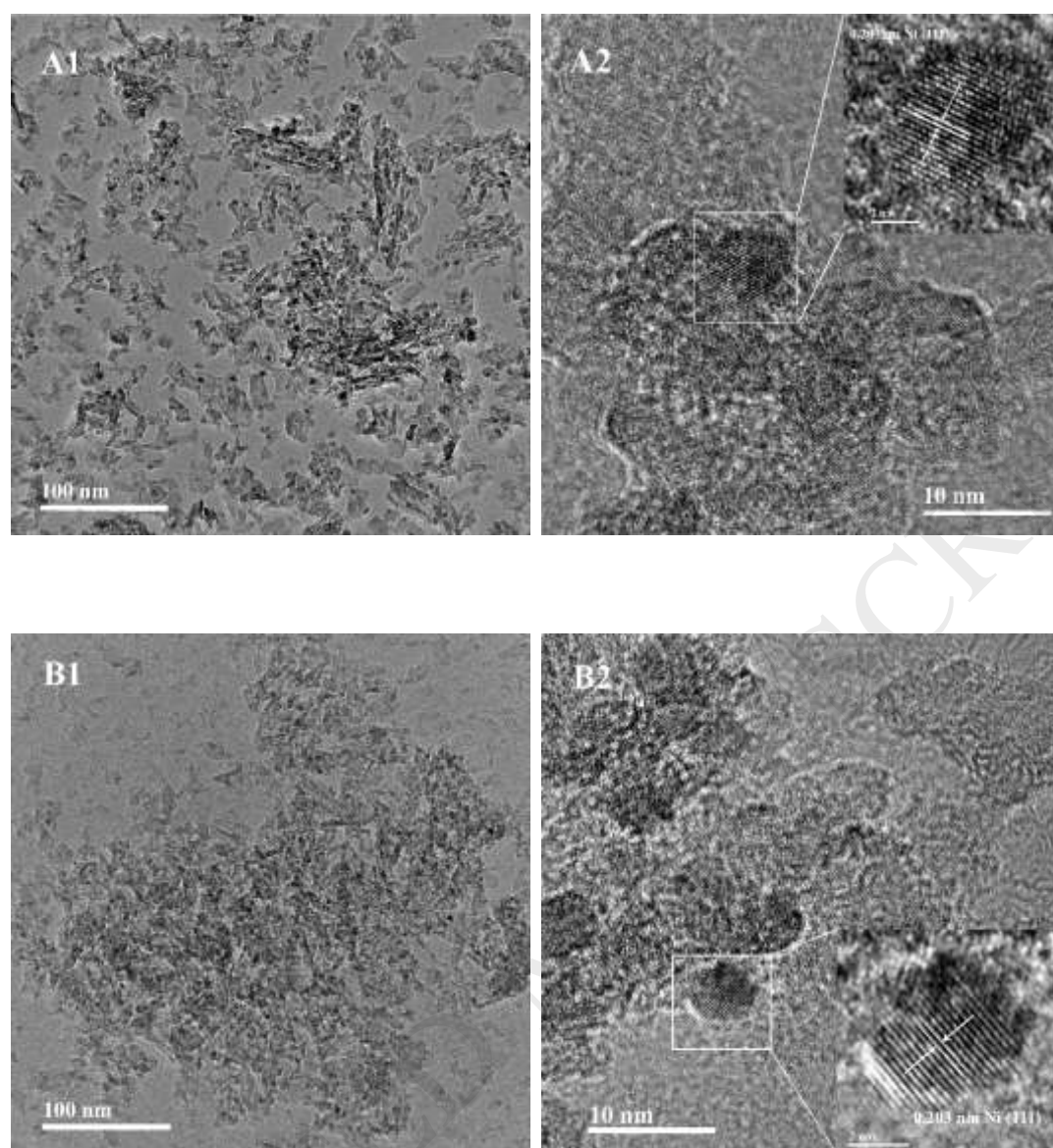


Fig. 3. HRTEM micrographs of Ni/γ-Al₂O₃ (A1-A2) and NiMo_{0.2}/γ-Al₂O₃ (B1-B2) catalysts.

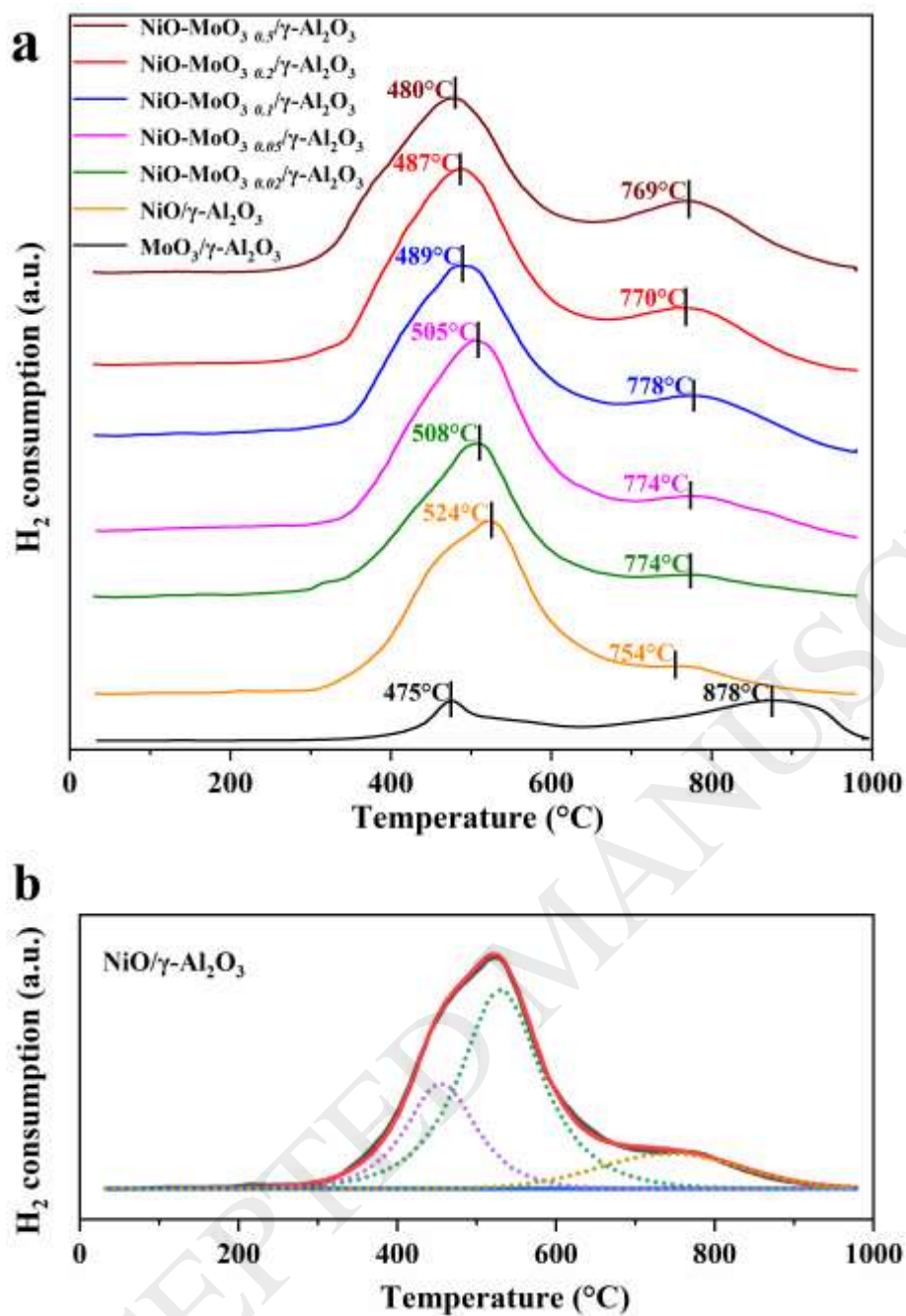


Fig. 4. TPR profiles of catalyst precursors MoO₃/γ-Al₂O₃ NiO/γ-Al₂O₃ and NiO-MoO_{3 X}/γ-Al₂O₃ (X = 0.02, 0.05, 0.1, 0.2 and 0.5) (a), deconvolution of the reduction curve of the NiO/γ-Al₂O₃ (b).

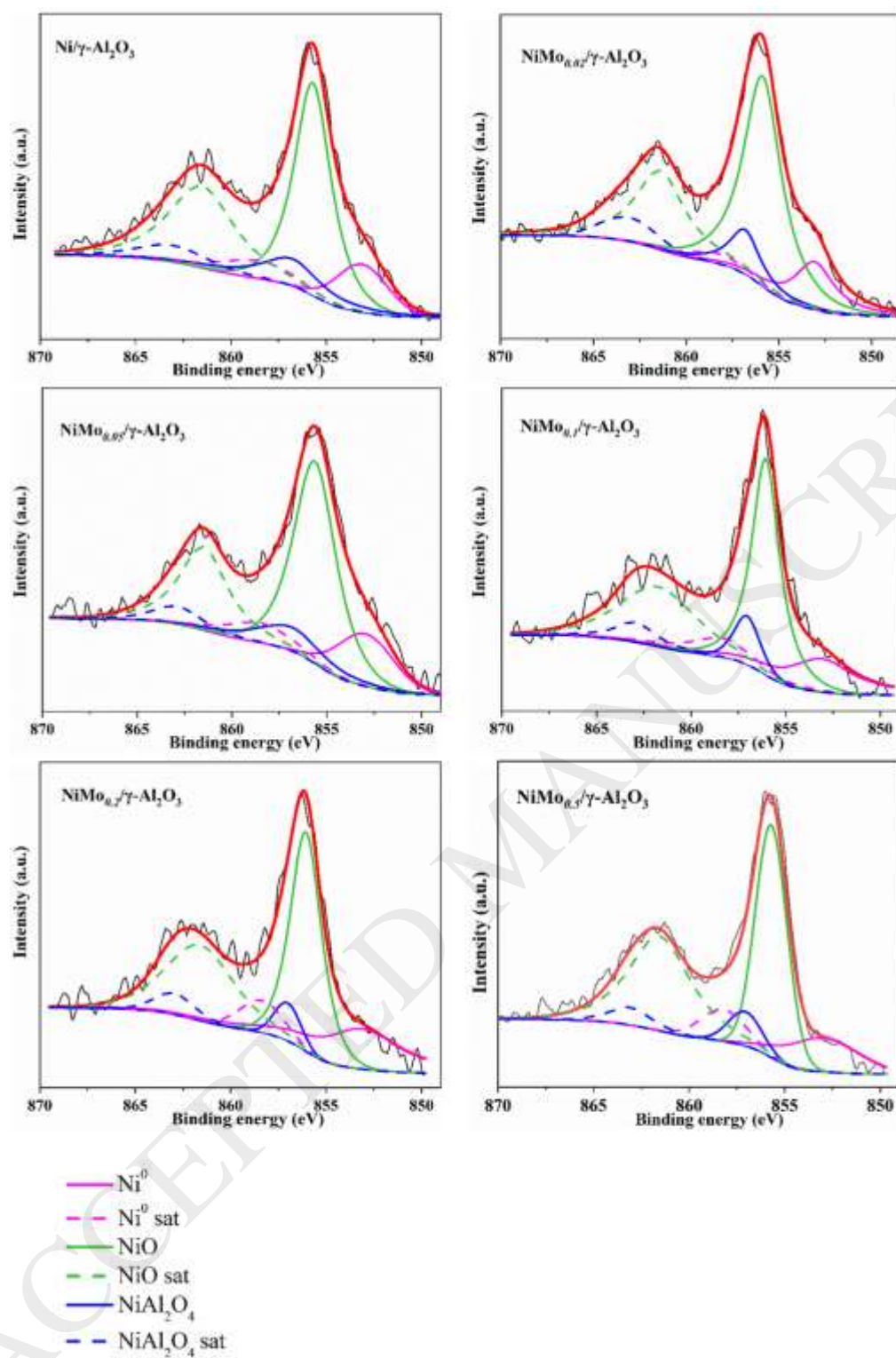


Fig. 5. Ni_{2p_{3/2}} XPS patterns of NiMo_X/γ-Al₂O₃ (X = 0.02, 0.05, 0.1, 0.2 and 0.5) and Ni/γ-Al₂O₃.

ACCEPTED MANUSCRIPT

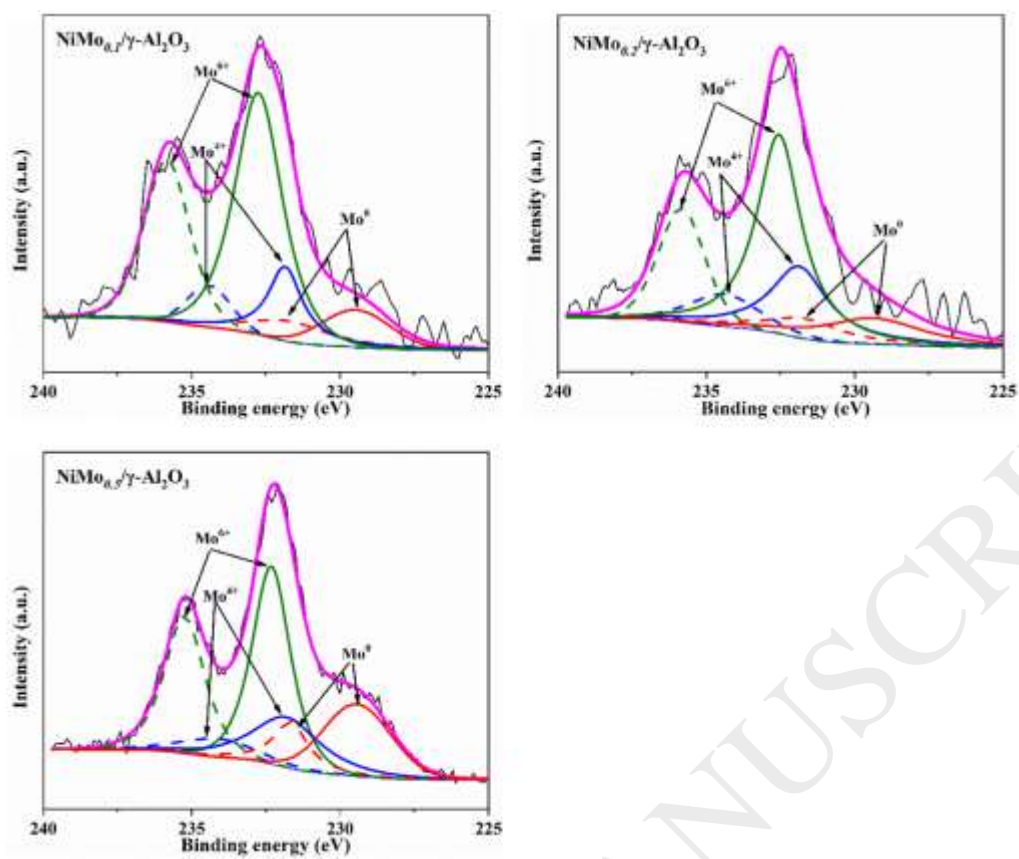


Fig. 6. Mo 3d XPS patterns of NiMo_{0.1}/γ-Al₂O₃, NiMo_{0.2}/γ-Al₂O₃ and NiMo_{0.5}/γ-Al₂O₃.

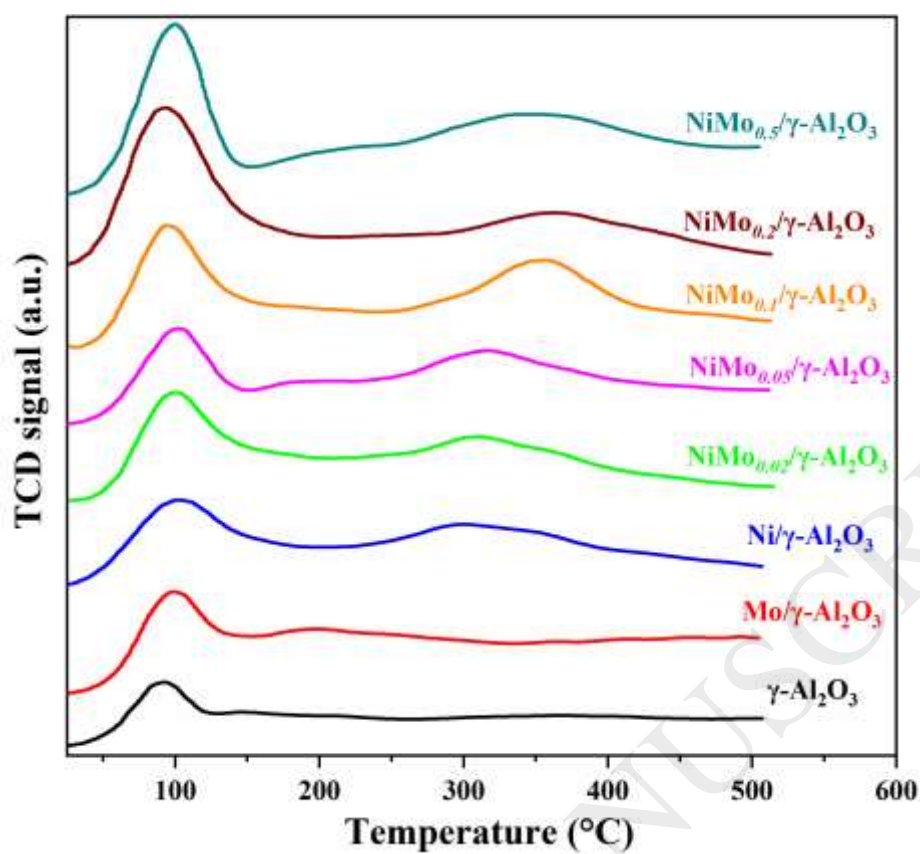


Fig. 7. DCPD-TPD profiles of $\text{NiMo}_x/\gamma\text{-Al}_2\text{O}_3$ ($X = 0.02, 0.05, 0.1, 0.2$ and 0.5), $\text{Ni}/\gamma\text{-Al}_2\text{O}_3$, $\text{Mo}/\gamma\text{-Al}_2\text{O}_3$ catalysts and $\gamma\text{-Al}_2\text{O}_3$ support.

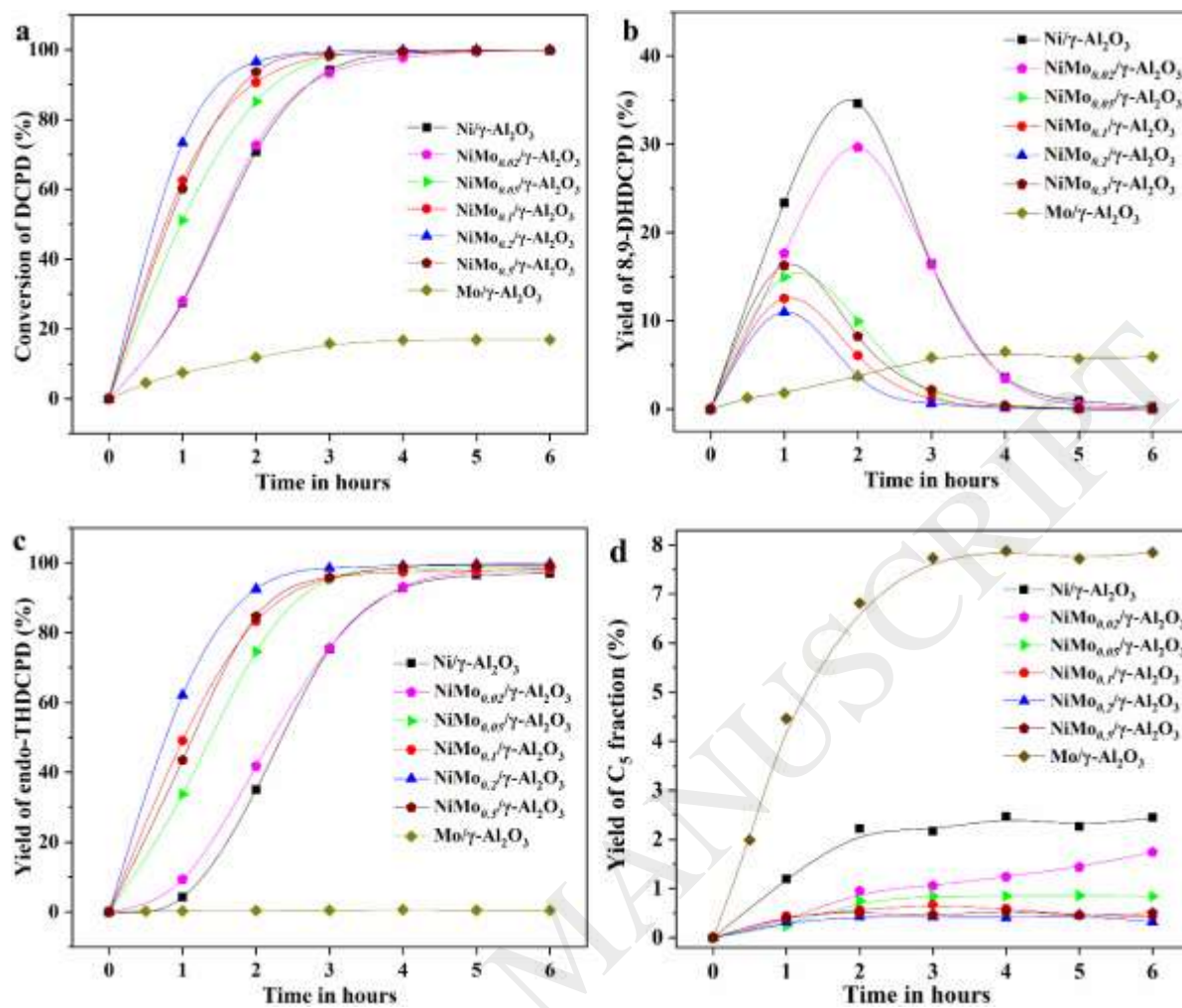


Fig. 8. Conversion of DCPD (a), yield of 8,9-DHDCPD (b), yield of endo-THDCPD (c) and yield of C₅ fraction (d) varying with reaction time (mass ratio of catalyst to DCPD to cyclohexane is 1:10:100; temperature 150 °C; hydrogen pressure 3.5 MPa; stirring rate 600 rpm)

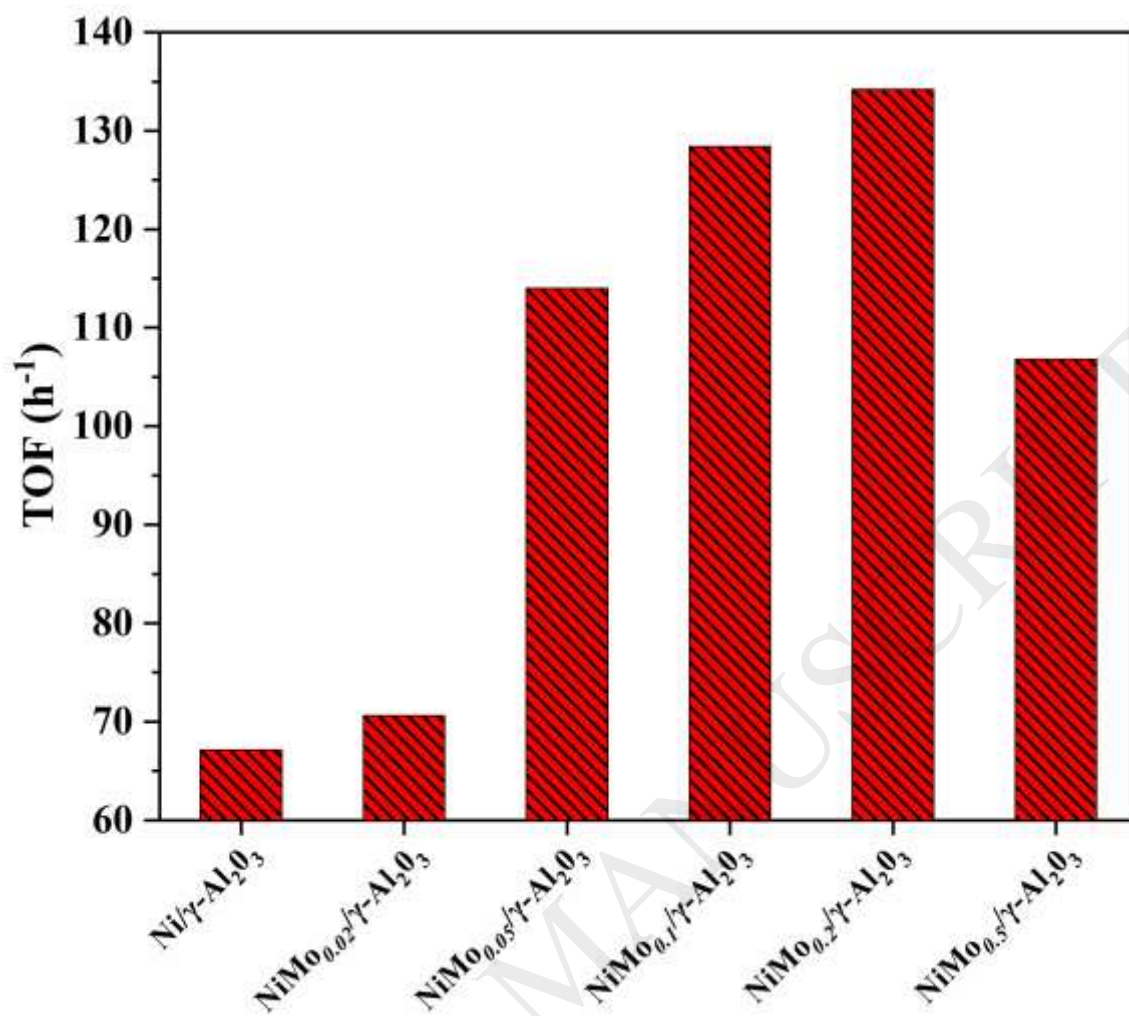


Fig. 9. Turnover frequency (TOF, h^{-1}) of various Ni-based catalysts for hydrogenation of DCPD